crystals

MDPI

Article

Supramolecular Assemblies of Melamine-2-Thiobarbiturate and Melamine-Barbiturate-2-Thiobarbiturate: Experimental and Theoretical Studies

Ivan V. Moskalenko [1], Vladimir V. Shilovskikh [1], Pavel V. Nesterov [1], Alexander S. Novikov [1], Malika Omarova [1], Roman V. Sadovnichii [1], Vladislav V. Gurzhiy [2], Nikita D. Orekhov [3,4,5] and Ekaterina V. Skorb [1,*]

[1] Infochemistry Scientific Center, ITMO University, Lomonosova Str. 9, 191002 Saint-Petersburg, Russia; moskalenko@infochemistry.ru (I.V.M.); vvshlvskh@itmo.ru (V.V.S.); nesterov@scamt-itmo.ru (P.V.N.); novikov@itmo.ru (A.S.N.); omarova@infochemistry.ru (M.O.); sadovnichii@infochemistry.ru (R.V.S.)
[2] Crystallography Department, Institute of Earth Sciences, Saint-Petersburg State University, University Emb. 7/9, 199034 Saint-Petersburg, Russia; vladislav.gurzhiy@spbu.ru
[3] Moscow Institute of Physics and Technology, Institutskiy per. 9, Dolgoprudny, 141701 Moscow, Russia; nikita.orekhov@phystech.edu
[4] Joint Institute for High Temperatures of the Russian Academy of Sciences, Izhorskaya Str. 13 Bd. 2, 125412 Moscow, Russia
[5] Department of Physics, Bauman Moscow State Technical University, FN-4, 2nd Baumanskaya Str. 5, 105005 Moscow, Russia
* Correspondence: skorb@itmo.ru

check for updates

Citation: Moskalenko, I.V.; Shilovskikh, V.V.; Nesterov, P.V.; Novikov, A.S.; Omarova, M.; Sadovnichii, R.V.; Gurzhiy, V.V.; Orekhov, N.D.; Skorb, E.V. Supramolecular Assemblies of Melamine-2-Thiobarbiturate and Melamine-Barbiturate-2-Thiobarbiturate: Experimental and Theoretical Studies. *Crystals* **2023**, *13*, 1302. https://doi.org/10.3390/cryst13091302

Academic Editors: Helmut Cölfen, Shujun Zhang, Jesús Sanmartín-Matalobos, Heike Lorenz and Sławomir Grabowski

Received: 21 July 2023
Revised: 15 August 2023
Accepted: 22 August 2023
Published: 25 August 2023

Copyright: © 2023 by the authors. Licensee MDPI, Basel, Switzerland. This article is an open access article distributed under the terms and conditions of the Creative Commons Attribution (CC BY) license (https://creativecommons.org/licenses/by/4.0/).

Abstract: In this work, we considered the formation of supramolecular assemblies of melamine-thiobarbiturate and melamine-barbiturate-thiobarbiturate. It is known that thiobarbituric acid can form many tautomers, as well as different motifs due to the change of C2=O to C2=S hydrogen bonds. We formed the crystal. The resulting crystals were studied with scanning electron microscopy (SEM), optical fluorescence microscopy, single crystal and powder (PXRD) X-ray diffraction analyses, and solid state nuclear magnetic resonance (ss NMR). These systems were theoretically studied using density functional theory (DFT) and classical molecular dynamics (MD) simulations. Interestingly, just as in the case of melamine barbiturate, during the crystallization process, hydrogen from the C5 moiety of thiobarbituric acid migrates to the melamine molecule. In addition, the resulting melamine thiobarbiturate crystals exhibit fluorescence behavior in the red region (~565–605 nm), while the melamine barbiturate crystals are fluorescent in the green region (512–542 nm).

Keywords: 2-thiobarbiturate acid; melamine-barbiturate; hydrogen bonds; supramolecular assembly; organic crystal; DFT; molecular dynamics

1. Introduction

An important role in supramolecular chemistry is played by hydrogen bonds between hydrogen atoms and electronegative elements and groups. This type of bond contributes to the formation of ordered molecular structures [1]. The formation of hydrogen bonds can be described as the transfer of hydrogen between a donor and an acceptor [2]. Oxygen or nitrogen often act as a hydrogen acceptor. On the other hand, it is of interest to study the formation of hydrogen bonds between other elements, such as sulfur or selenium [3]. Studies show that the formation of hydrogen between sulfur and hydrogen leads to the formation of many structural motifs [4,5].

Thiobarbituric acid (TBA), barbituric acid (BA), and melamine (M) formulas are shown in Figure 1. TBA is well known as one of the reagents used for determining lipid peroxidation [6]. The presence of an acidic proton in the C5 position in its structure makes it a convenient substrate for various modifications, including amination [7] and

Knoevenagel [8–14] reactions; at the same time, the presence of sulfur in the structure makes it possible to form complexes with metals [15,16], and the presence of carboxyl and amine groups allows the formation of intermolecular hydrogen bonds, which could be utilized to create multimodal supramolecular polymers with desired properties [17,18] and control crystallization [19].

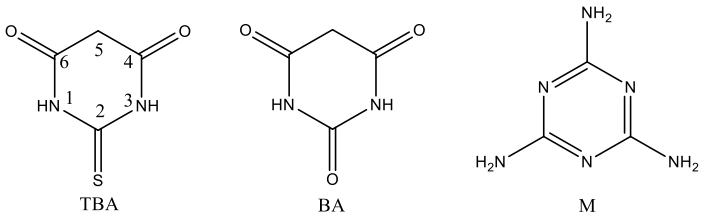


Figure 1. Structures of parent compounds.

Another important property of TBA is the presence of many tautomeric forms [12,20,21]. Five tautomeric forms were experimentally observed out of ten theoretically possible [12]. In addition, it is known that the most thermodynamically favorable structures of TBA can form cocrystals [21] and deposit on the surface of gold nanodots [22,23].

BA and cyanuric acids have a similar structural motif to TBA. For these compounds, supramolecular assemblies with M are known [24–32]. Despite their similar spatial shape, these acids form different co-crystals with M. M cyanurate forms monoclinic crystals with the space group I2/m, composed of flat two-dimensional layers with a threefold rotation axis [33], while for M-BA the symmetry space group was defined as Ccc2 [29]. The crystal is composed of endless flat ribbons with alternating M and BA molecules arranged one above the other. Electrostatic bonds play an important role in the stabilization of this crystal [29]. Surprisingly, self-assemblies of melamine and TBA have not been reported, and this work intended to fill the corresponding gap in the supramolecular chemistry of TBA.

2. Materials and Methods

2.1. Reagents

Melamine (M) ($C_3H_6N_6$, 99.0%, Sigma Aldrich, St. Louis, MO, USA), barbituric acid (BA) ($C_4H_4N_2O_3$, 99.0%, Sigma Aldrich), and agar-agar were purchased at Sigma Aldrich; 2-tiobarbituric acid (TBA) ($C_4H_4N_2O_2S$,98.0%, Lenreactiv, St. Petersburg, Russia) was purchased at Lenreactiv. All the solutions were prepared using Millipore Elix, Burlington, Columbus, NJ, USA (18 MΩ·cm^2/cm) deionized water.

2.2. Sample Preparation

Samples of crystalline M-BA containing TBA were prepared by mixing 20 mM solutions of either M or BA containing similar concentrations of TBA.

M-TBA crystals were obtained by mixing 20 mM solutions of M and TBA. Next, about 80% of the liquid was evaporated and left to crystallize until pink crystals precipitated.

Then, the supernatant liquid of the powder precipitate was decanted, and the remaining powder was centrifuged and washed three times with water. Finally, the powder was dried.

The diffusion-controlled samples were prepared as follows. Agar-agar gel was laid out in a Petri dish, while a third of the volume was occupied by a gel prepared based on a 20 mM solution of M, and a gel prepared based on a 20 mM solution of BA was in the other half. A 20 mM TBA solution was added to the central space not occupied by the gel. Three days later, the resulting precipitate was filtered.

2.3. Microluminescence Spectra

Microluminescence spectra of solid-state M-TBA crystals were acquired using a Zeiss Axio Imager, A2m, equipped with an Ocean Optics QE Pro spectrometer (St. Petersburg, Russia) (excitation by HAL 100 and HBO 100).

2.4. Microscopy

Scanning electron microscopy (SEM) and electron dispersion X-ray (EDX) studies were performed with a Hitachi S-3400N scanning electron microscope (Tokyo, Japan) and Oxford X-Max 20 EDX spectrometer (Abingdon, UK). EDX analysis was performed at 5 kV accelerating voltage and 0.2 nA beam current, to increase the locality of the method.

Optical photos were acquired with a Leica 4500P (Wetzlar, Germany) equipped with halogen UV-source and luminescence filters: DAPI (325–375 nm excitation, 435–485 nm emission), FITC (460–500 nm excitation, 512–542 nm emission), and RHOD (541–551 nm excitation, 565–605 nm emission).

2.5. Powder X-ray Diffraction

Powder X-ray diffraction (PXRD) measurements of M-BA-TBA powder were performed on a Bruker D2 (Karlsruhe, Germany) with Cu Kα radiation from diffractionless silicon as a special substrate for the sample, with a speed of 1 degree per minute. All calculations for power XRD were made using regular Topas software (version 6.0).

2.6. Single Crystal X-ray Diffraction

Single crystal X-ray diffraction (XRD) studies were performed at 100 K using an XtaLAB Synergy-S diffractometer (Rigaku Oxford Diffraction, Oxford, UK) equipped with a hybrid photon counting HyPix-6000 detector that was operated with monochromated, microfocused CuKα radiation (λ[CuKα] = 1.54184 Å) at 50 kV and 1.0 mA. The data obtained were processed and normalized for polarization, Lorentz, and background effects. The CrysAlisPro [34] program was utilized to perform an empirical absorption correction based on spherical harmonics implemented in the SCALE3 ABSPACK algorithm. The unit-cell parameters were obtained via refining using the least-squares algorithms. The SHELX program [35,36] incorporated in the OLEX2 program package [37] was applied to refine the structure previously solved using a dual-space algorithm. The finalized model incorporated coordinates and anisotropic displacement parameters for all non-hydrogen atoms. The coordinates of carbon-bound hydrogen atoms were found from different Fourier maps and were included in the refinement without any restraints with individual isotropic displacement parameters (see Supplementary Materials).

2.7. Solid-State Nuclear Magnetic Resonance

The cross polarization/magic-angle spinning (CP-MAS) and cross polarization polarization inversion (CPPI) nuclear magnetic resonance spectra (NMR) were recorded (at 292 $\pm$ 1 K) on a Bruker AMX-400 (Rheinstetten, Germany) instrument operating at 7.05 T. The MAS rate was 8 kHz. Acquisition was performed with a standard CP pulse sequence using a 3.5 µs proton 90° pulse, a 800 µs contact pulse, and a 2.5 s delay between repetitions.

2.8. Quantum Chemical Computations

The full geometry optimization for all model structures was carried out at the B3LYP-D3/def2-SVP level of theory with the help of the Orca 5.0.3 program package [38]. The RIJCOSX approximation [39,40] utilizing the def2-SVP/C auxiliary basis set and spin restricted approximation were employed. The convergence tolerances for the geometry optimization were energy change = 5.0×10^{-6} Eh, maximal gradient = 3.0×10^{-4} Eh/Bohr, RMS gradient = 1.0×10^{-4} Eh/Bohr, maximal displacement = 4.0×10^{-3} Bohr, and RMS displacement = 2.0×10^{-3} Bohr. The couple perturbed self-consistent field (CPSCF) equations were solved using the conjugated gradient (CG) method, with convergence tolerance on a residual of 1.0×10^{-6} Eh. The solvent effects were taken into account by the SMD model [41]. The Hessian matrices were calculated for all optimized model structures, to determine the location of the correct stationary points on the potential energy surfaces (no imaginary frequencies were found in all cases) and to estimate the thermodynamic properties (Gibbs free energy) for all model systems at 298.15 K and 1 atm. Cartesian atomic coordinates of all model structures are presented in the Supplementary Materials.

2.9. Molecular Dynamics Simulation Details

Molecular dynamics simulations of M-TBA and M-BA-TBA were performed utilizing the GROMACS program package version 2021.4 [42]. Interatomic interactions were described by the OPLS-AA/CM1A force field [43] with topology and charges generated by LigParGen [43–45]. For the water model, a rigid non-polarizable TIP3P [46] model was used. The cut-off for non-bonded and long-range interactions was 1.2 nm. For the calculation of long-range Coulomb interactions, the Particle-Mesh Ewald was used [47]. Energy minimization was performed with the steepest descent algorithm. Simulations were performed in the NPT ensemble at T = 300 K and P = 1 atm in the cubic unit cell (approximate size 85 × 85 × 85 A^3). The integration timestep for the trajectory calculations was 2 fs, and for relaxation 0.5 fs. Spatial distribution functions and dimer existence autocorrelation functions were calculated from the resulting trajectories using the TRAVIS program package version 21 May 2021 [48].

3. Results and Discussion

Since TBA can form different tautomers [12,15,49], we evaluated through quantum chemical calculations the Gibbs free energies of all possible tautomeric forms in the gas phase and aqueous solution (Figure 2a,c). Solvation reduces the relative Gibbs energy of formation. The difference between the most thermodynamically favorable (viz. TBA1 and TBA10) forms of TBA is 27.5 kJ/mol, thus it is clear that TBA1 prevails in the aqueous solution. However, one should not exclude the possibility of ketone-enol isomerization during the formation of crystals [21]. The calculation of TBA-M dimers (Figure 2b) showed that the formation of the M-TBA7 dimer (ΔG = −47.66 kJ/mol) is most beneficial, which is much more profitable than the formation of the BA-M dimer (ΔG = −40.9 kJ/mol) [29]. However, the geometry of this dimer does not fit into the structure determined by single crystal XRD. In addition, all TBA(**9–10**) tautomers are unsymmetrical, which reduces the likelihood of symmetrical patterns being formed.

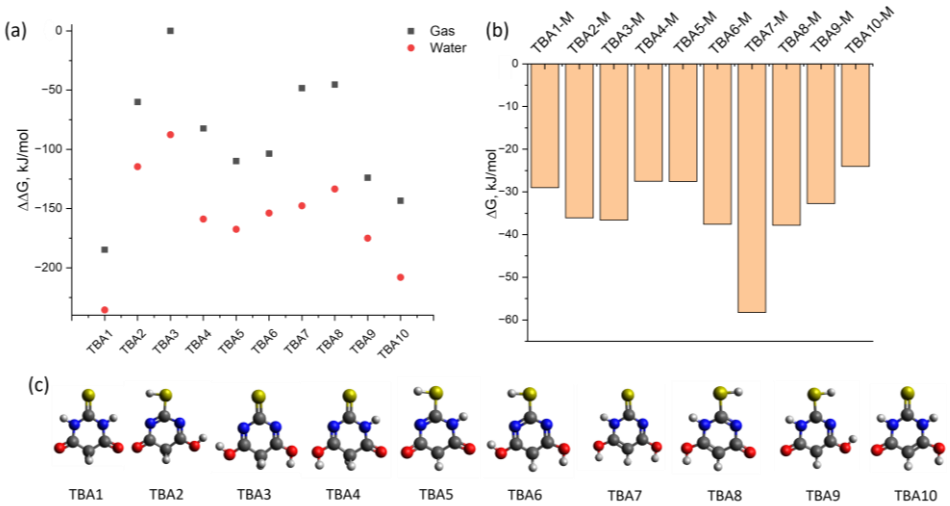


Figure 2. (**a**) Calculated Gibbs energy of the TBA tautomers in the gas phase and in aqueous solution. (**b**) Gibbs energy of formation of M-TBA dimers. (**c**) Optimized structures of TBA tautomers in the gas phase.

The calculation of the energy of the formation of dimers and trimers M-(BA)-TBA1 is shown in Figure 3. The least thermodynamically favorable is the formation of a dimer (compound **1**, Figure 2a). In this case, the Gibbs energy of dimer formation (**1**) practically coincides with the Gibbs energy of the formation of a similar M-BA dimer, which indicates the absence of a noticeable effect of sulfur on the formation of hydrogen bonds between carboxyl groups and -NH_2 of melamine. Compared to the BA-M dimer [29], the formation of M-TBA1 (compound **2**) is less favorable (−27.00 kJ/mol), while the distance between the

sulfur atoms in TBA and the hydrogen atom in melamine is 2.382 Å rather than 1.877 Å for a similar bond in the case of M-BA, and the length of the hydrogen bond between the NH_2 of melamine and the carboxyl group of TBA1 is reduced to 1.839 Å (in the case of BA-M, the bond is 1.874 Å). Thus, the M and TBA molecules in this dimer are not in the same plane. The formation of trimer (**5**) turned out to be slightly more thermodynamically favorable than trimers (**3**) and (**4**). The trimer consisting of M-BA-TBA1 molecules (**6**) has a calculated Gibbs energy of formation equal to −65.97 kJ/mol, which indicates the possible incorporation of TBA into the M-BA structure. The decrease in Gibbs free energy during the formation of M-TBA1 aggregates, as compared to M-BA, can be attributed to the lower energy negativity of sulfur relative to oxygen [50,51].

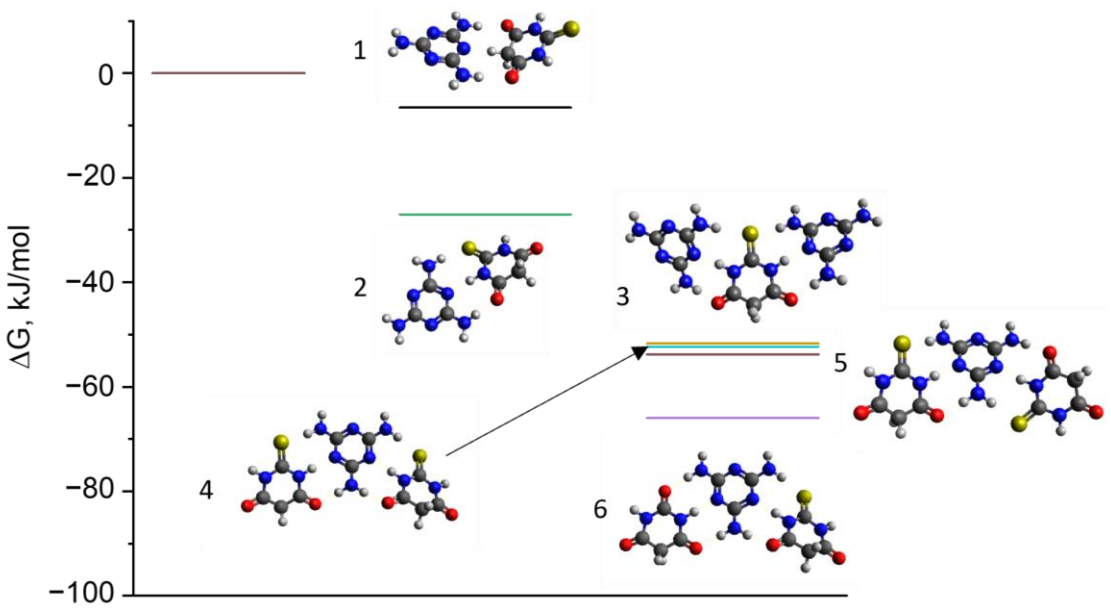


Figure 3. Change in Gibbs free energy of association during the formation of M-TBA and M-BA-TBA supramolecular assemblies with respect to initial components.

To gain insight into the first stages of the formation of M-TBA with and without inclusion of BA, we utilized classical molecular dynamics simulations. We performed simulations of two systems: M-TBA (40-40 molecules per 85 $Å^3$) and M-BA-TBA (40-20-20 molecules per 85 $Å^3$). The final analysis of equilibrated trajectories is represented in Figures 4 and 5.

Figure 4 shows radial distribution functions (RDF), dimer existence autocorrelation functions (DACF), and neighbor counts for M-TBA and M-BA systems. Figure 4a depicts RDF for the intermolecular bonds between the H(N) atom of TBA and N atom of M. We can conclude that the most intense peak on the graph is at approximately 1.9 Å, which is in correspondence with the average length of the hydrogen bond between TBA and M. Alternatively, Figure 4b shows the RDF for intermolecular bond between S atom of TBA and H(N) atom of M. There are no peaks at the distance corresponding to hydrogen bonds. Therefore, all hydrogen bonds between M and TBA molecules are represented by H(N)-TBA and N-BA hydrogen bonds. Figure 4c shows the DACF for system with and without BA molecules—in other terms the lifetime of the M-TBA dimers. The inclusion of BA molecules in the system slightly decreases the lifetime of M-TBA dimes, due to the competitive process of M-BA dimer formation. Figure 4d,e depicts the neighbor count of M-TBA for the M-BA-TBA system and M-TBA system, respectively. There are almost no changes in the neighbor count for systems with and without inclusion of BA.

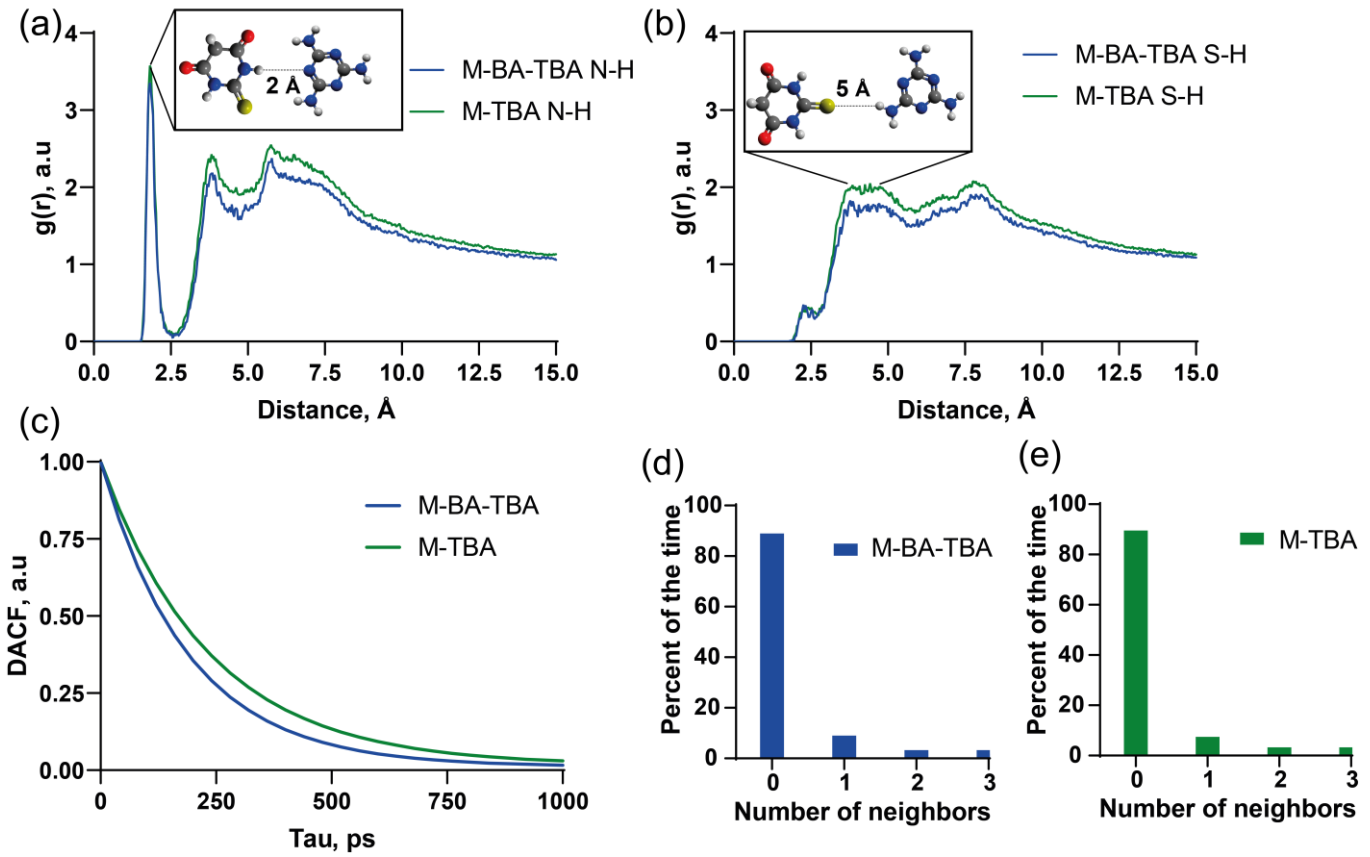


Figure 4. (**a**) Radial distribution functions between N atom of M and H(N) atom of TBA for systems with (blue line) and without (green line) inclusion of BA molecules; (**b**) radial distribution functions between H atom of M and S atom of TBA for systems with (blue line) and without (green line) inclusion of BA molecules; (**c**) dimer existence autocorrelation functions for M-TBA for systems with (blue line) and without (green line) inclusion of BA molecules; (**d**,**e**) number of neighbors for M-TBA dimers for systems with (blue columns) and without (green columns) inclusion.

Data in Figure 5a,b,d,e represent the spatial distribution function between M and TBA molecules with and without the inclusion of BA molecules. For both types of systems one can conclude that the M-TBA dimer forms both by π–π stacking and hydrogen bonds. In correspondence with the RDF data, the hydrogen bonds only form between the H(N) atom of TBA and N atom of M.

The most significant change between the M-BA-TBA and M-BA systems is represented in Figure 5c (without the inclusion of BA) and Figure 5f (with the inclusion of BA). The time-dependent radial distribution function between M and TBA depicted in Figure 5c,f shows the dynamics of early-stage nucleation. The wider the area on the horizontal (distance) axis, the bigger the nuclei; the larger the area on the vertical (time) axis, the greater the lifetime of a nuclei. This shows that the inclusion of BA molecules in the system suppresses the formation of M-TBA nuclei.

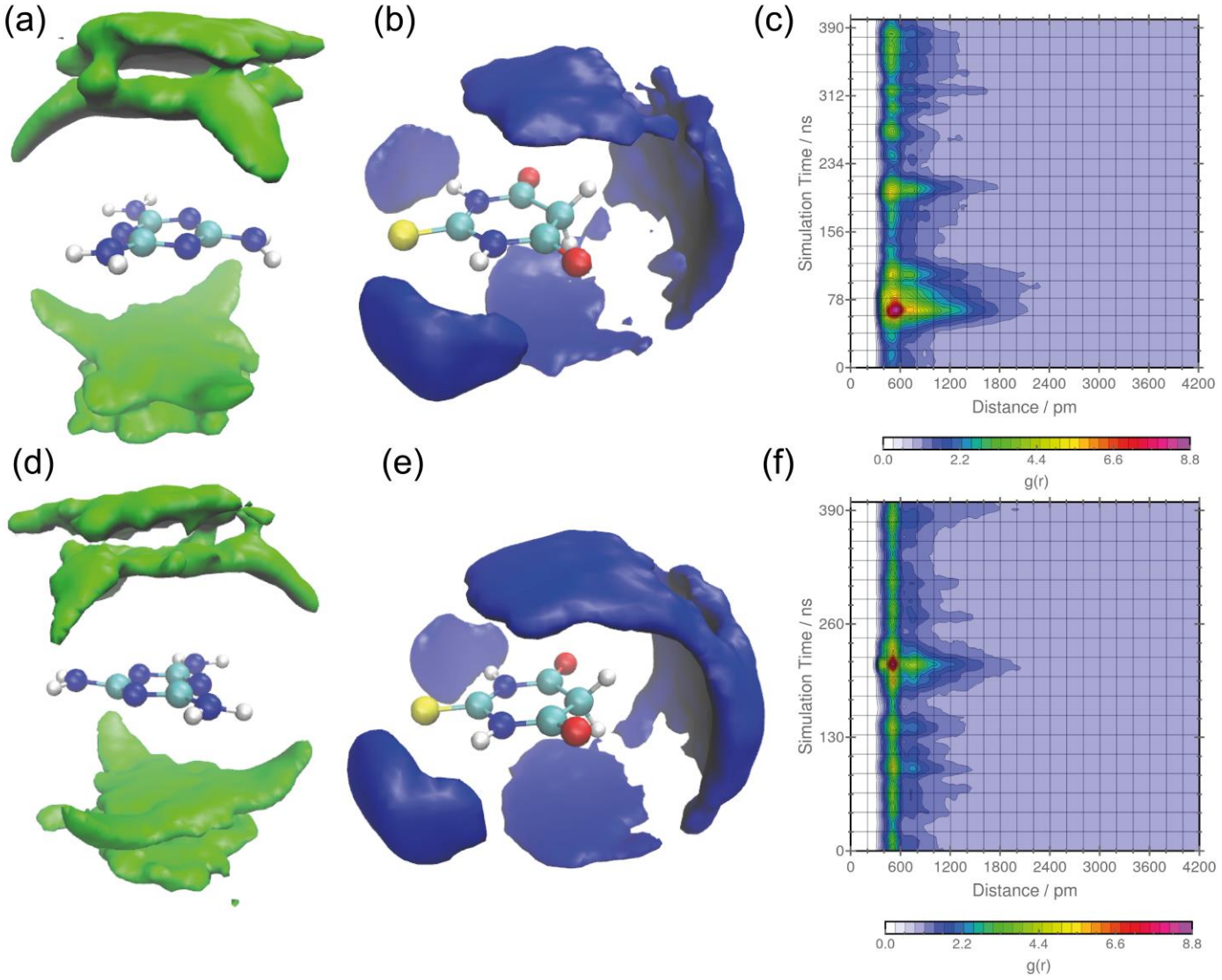


Figure 5. Spatial distribution functions for TBA around M without (**a**) and with (**d**) inclusion of BA in the system, spatial distribution functions for M around TBA without (**b**) and with (**e**) inclusion of BA in the system. Time-dependent radial distribution function between centers of mass of M and TBA molecules for systems without (**c**) and with (**f**) BA.

The data from the theoretical calculations were also confirmed experimentally: at room temperature, the self-assembly of thiobarbiturate and melamine did not form spontaneously from saturated solutions of TBA and M. To obtain M-TBA crystals, a solution containing 10 mmol of TBA and 10 mmol of M was boiled, evaporating 80% of the water. At the same time, no visible signs of crystal precipitation were observed; on the second day, rhombic crystals precipitated, which could be identified as melamine crystals. A few days later, pink crystals precipitated, having a lamellar structure (Figure 6a); less often "hedgehogs" and fluorescing in the DAPI and RHOD ranges (Figure 4a). At the same time, M-BA fluoresced in the DAPI and FITC ranges [30]. From the SEM images (Figure 6b), M-TBA had a layered structure, and the EDX analysis showed the sulfur content in the sample (Figure 6c). Recrystallization of M-TBA crystals from ethanol formed rose-type structures, the dimensions of which were much smaller than those of the M-TBA crystals formed in water. As well as the crystals obtained from an aqueous solution, these agglomerates had fluorescence in the DAPI and RHOD ranges.

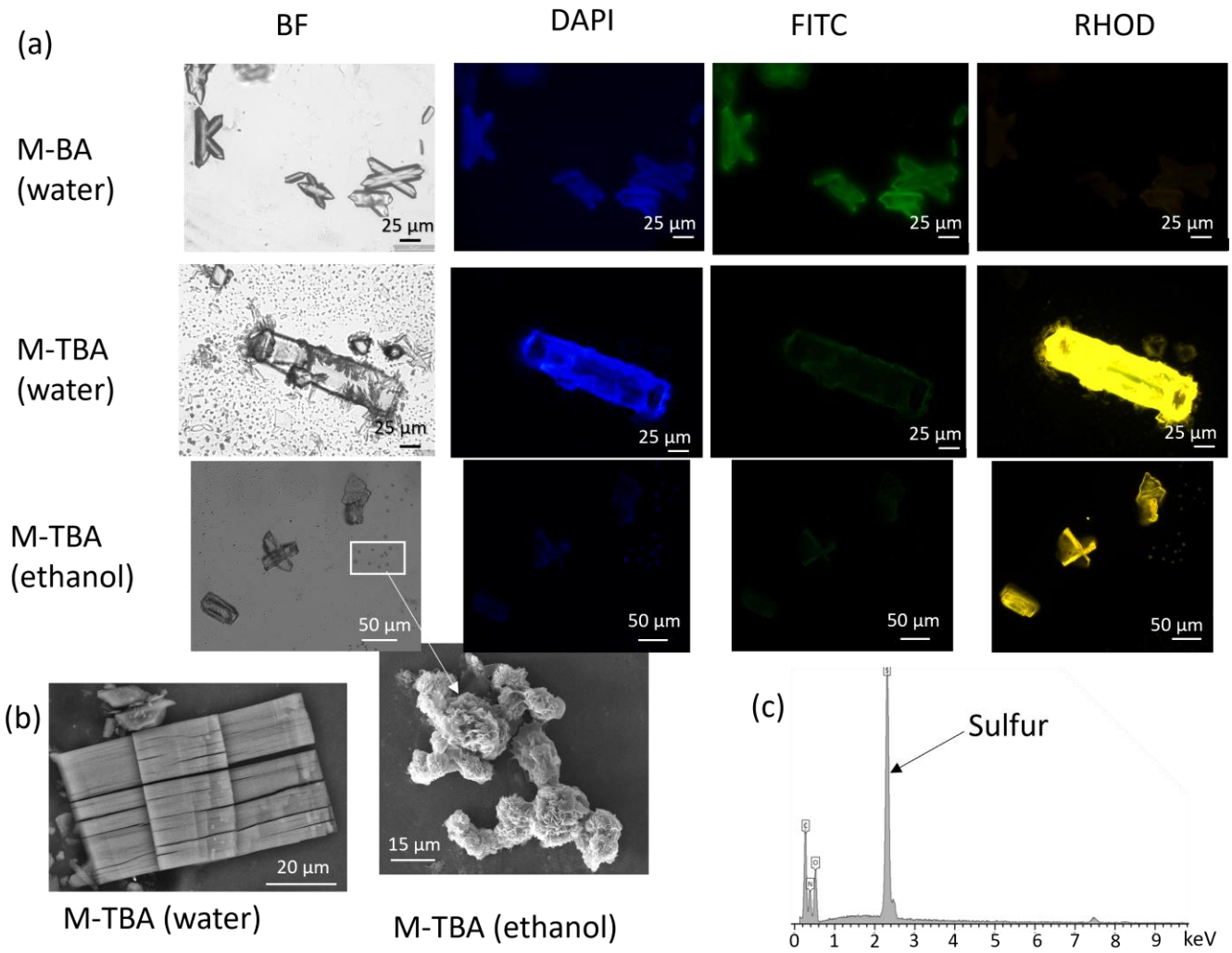


Figure 6. (**a**) Photomicrographs of crystal in daylight and fluorescent channels. (**b**) SEM photographs of TBA-M crystals. (**c**) EDX analysis of TBA-M crystal.

Of the starting compounds, only M exhibited noticeable fluorescence. Thus, it can be assumed that fluorescence in this system can arise for four reasons: (1) fluorescence due to the transition to another tautomeric form in the excited state [52,53]; (2) hydrogen atom transfer from TBA to M; (3) fluorescence of radical species; and (4) fluorescence on crystal defects [54].

We succeeded in isolating and characterizing a single M-TBA crystal. The parameters and volume of the crystal cell are shown in Table 1. Only one tautomeric form of TBA was found in the studied crystal. Apparently, this is because the TBA1 tautomer predominates in the aqueous phase. In the crystal structure of TBA-M, TBA and M molecules are combined into dimers of two types, through three type of hydrogen bonds: N–H. . .O (2.78 Å), N–H. . .N (3.09 Å), and N–H. . .S (3.29 Å) (Figure 7a). Dimers are similar in composition and the structure differs only in the location geometry. The dimers alternate and combine directly through N–H. . .S (3.27 Å) and N–H. . .O (2.83 Å) hydrogen bonds, forming two types of ribbons (highlighted in blue and orange in Figure 7a). The ribbons are connected to each other into layers by N–H. . .O (2.93, 2.79, and 2.93 Å) and O–H. . .O (2.79 Å) hydrogen bonds through water molecules. These layers correspond to the (10-2) plane. Water molecules are linked by hydrogen bonds (O–H. . .O) with a length of 2.78 Å. The layers are also connected to each other through water molecules by hydrogen bonds of the O–H. . .O type, 2.73 and 2.79 Å long (Figure 7b). Thus, the cracks in the SEM images (Figure 6b) can be associated with the release of water from the structure during the vacuumization of the sample.

Table 1. Parameters and volume of the monoclinic cell for M-TBA.

	Space Group	*a*, Å	*b*, Å	*c*, Å	*β*, °	*V*, Å^3
M-TBA	P 2_1/c	10.7987 (3)	17.7255 (4)	6.7670 (2)	90.698 (3)	1295.19 (6)

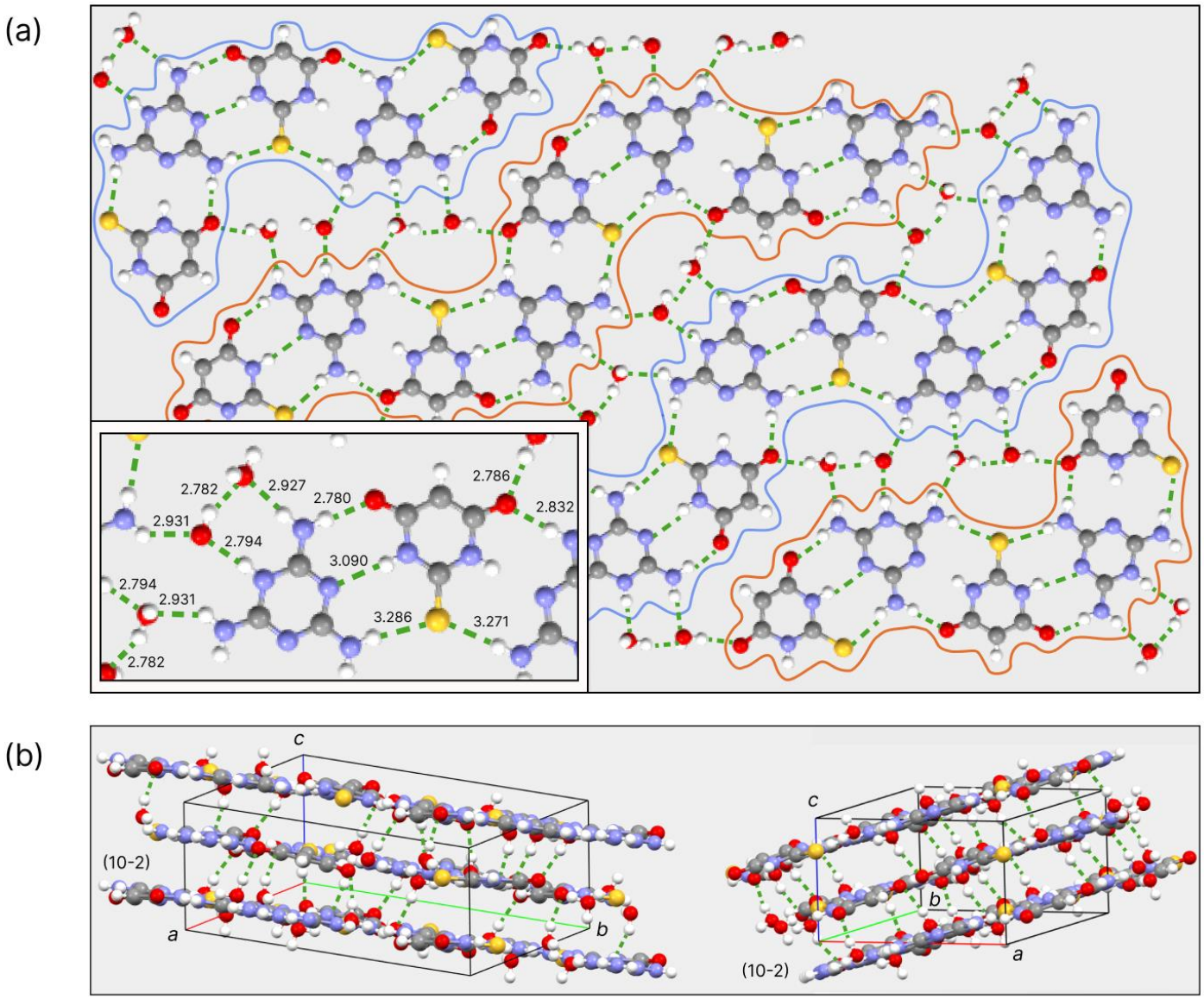


Figure 7. (**a**) Projection of crystallographic plane (10-2). (**b**) Volumetric M-TBA structure. Distance is in Å. Yellow atoms—sulfur, gray—carbon, purple—nitrogen, white—hydrogen.

As in the case of M-TBA, hydrogen connected with C5 passes from the CH_2 group of TBA to the M molecule. However, a more accurate confirmation of the transition of hydrogen would be the application of such methods as X-ray photoelectron spectroscopy (XPS) and solid-state nuclear magnetic resonance [55,56]. The Supplementary Materials show (Figure S3) the spectra of CP-MAS and CPPI. No negative signals are observed in the CPPI spectra, which indicates the absence of CH_2 groups in the crystals.

Using the PXRD method, it was established (Figure 8) that the structure of these supramolecular assemblies coincided with the initial M-BA. At the same time, with an increase in the concentration of TBA, the crystallinity parameter decreased. Samples obtained by diffusion control had the highest crystallinity. However, the lattice parameters differed slightly in M-BA, and the volume of the crystal lattice increased from 971.9 $Å^2$ to 1006.7 $Å^2$. Apparently, this was due to an increase in the distance, due to the complexity of the formation of a hydrogen bond between the TBA sulfur and the hydrogens of the melamine amino groups. Thus, TBA changes the morphology and shape of M-BA crystals.

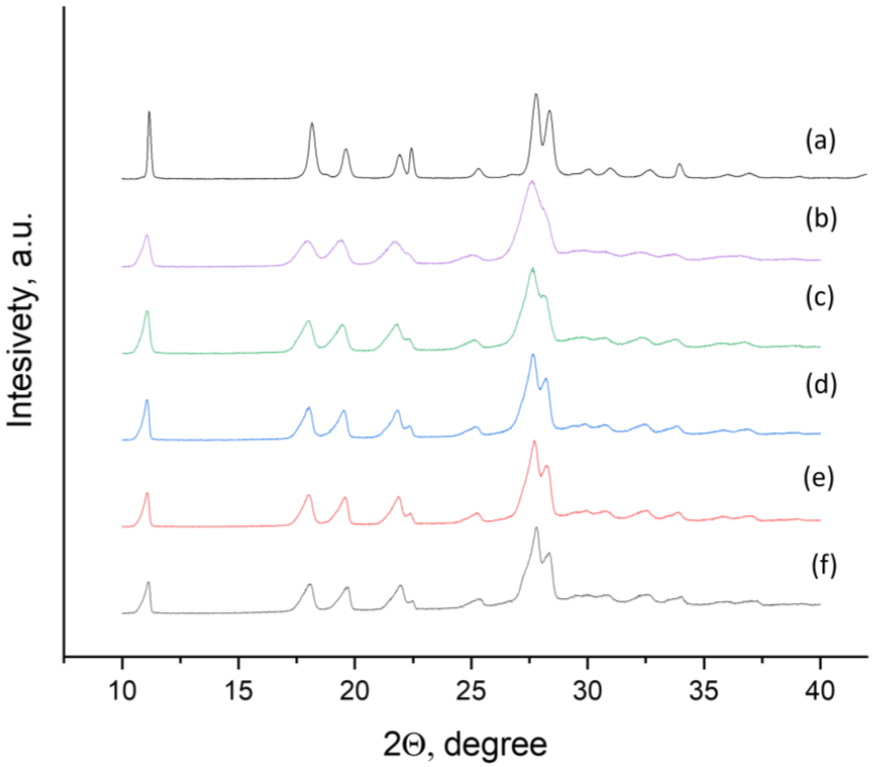


Figure 8. Powder XRD patterns for M-BA-TBA and M-BA crystals with different concentrations M:BA:TBA (a) 20 mM:20 mM:20 mM (under diffusion-controlled conditions) (b) 20 mM:20 mM:15 mM; (c) 20 mM:20 mM:7.5 mM; (d) 20 mM:20 mM:5 mM; (e) 20 mM:20 mM:2.5 mM; (f) M-BA crystals.

As we noted earlier, it follows from quantum chemical calculations and molecular dynamics modeling that TBA will be incorporated into the structure of the M-BA crystal ribbon. M-BA-TBA crystals obtained by adding low concentrations of TBA have the form of melamine barbiturate crystals with defective twin growth points, at high concentrations the shape of "hedgehogs", the "needles" of which have the shape of a hexagonal prism topped with a triangular pyramid head. Upon receipt of melamine-barbiturate-thiobarbiturate under diffusion control, hexagonal crystals grow (Figure 9).

All crystals glow in fluorescent channels (RHOD, FITC, and DAPI). The EDX spectrum shows the presence of sulfur in the sample (Supplementary Materials).

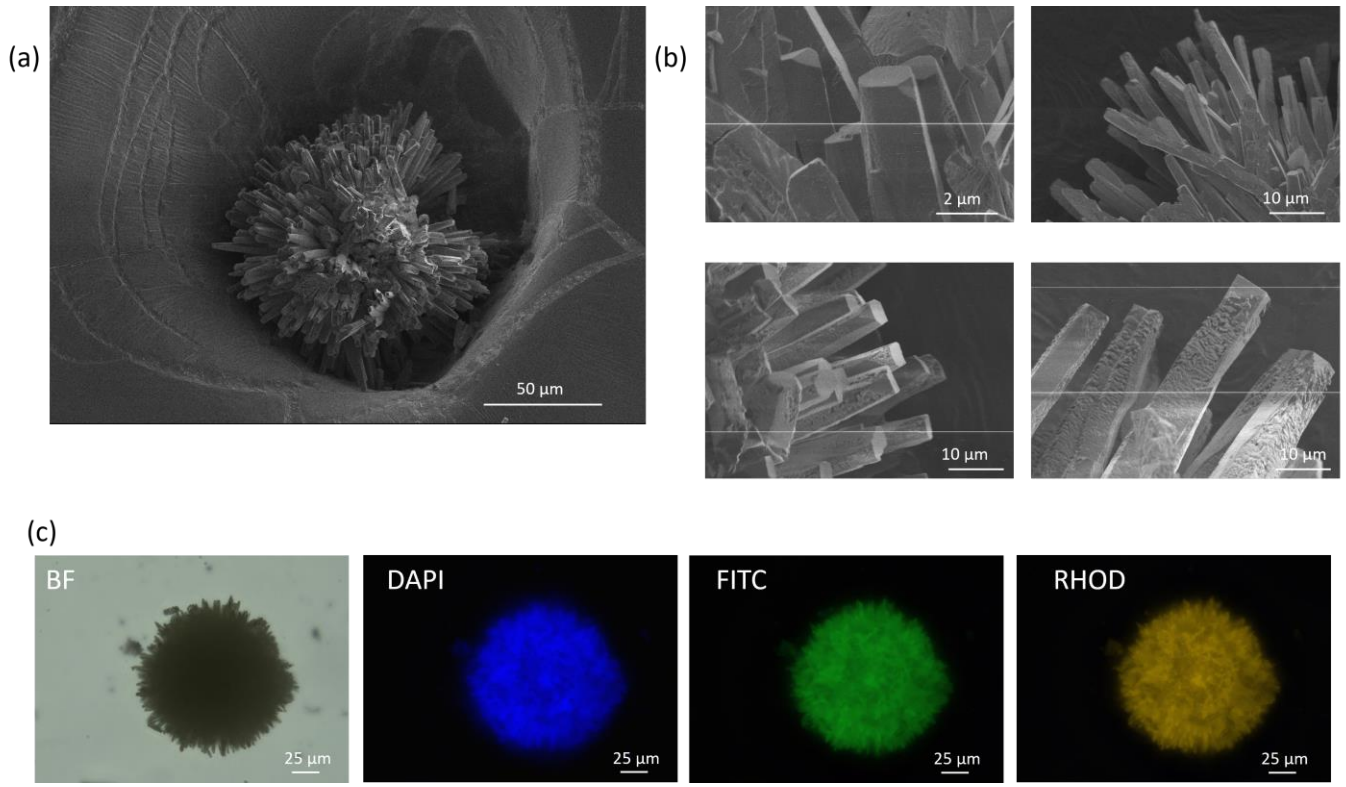


Figure 9. (**a**,**b**) SEM image M-BA-TBA crystal, (**c**) Microscopy image M-BA-TBA in bright-field mode and fluorescent filters.

4. Conclusions

In conclusion, in this work, the supramolecular assemblies of M and TBA were studied theoretically (DFT and MD) and experimentally (single crystal XRD, ss-NMR, SEM, EDX), and the possibility of embedding TBA into M-BA was shown. The obtained crystal structure of M-TBA does not have tautomeric forms in its structure, except for TBA1. The crystalline cell is layered, while the layers are interconnected using hydrogen bonds that are part of the structure of water molecules. Sheets consist of ribbons alternating M and TBA, as well as water. At the same time, the motif of the structure was in good agreement with the theoretically calculated TBA-M-TBA trimer (compound **5**, Figure 3). From a molecular dynamics point of view, M-TBA is predominantly formed through π-π stacking and hydrogen bonds between H(N) atom of TBA and N atom of M. Moreover, the inclusion of BA molecules in the system led to slower formation of M-TBA nuclei.

It is interesting that, as in the case of M-BA, M-TBA crystals have a fluorescence shifting towards RHOD. We hypothesized the following structure-based causes of fluorescence: (1) fluorescence due to the transition to another tautomeric form in the excited state; (2) proton transfer from TBA to M; (3) fluorescence due to radicals contained in the crystal structure; and (4) fluorescence on crystal defects. The incorporation of TBA into M-BA crystals leads to a decrease in crystallinity, apparently since the TBA molecule becomes a source of a defect, resulting in structure twinning. In this case, the crystal cell remains the same. The resulting M-BA-TBA crystals have the shape of "hedgehogs", and the crystal cell repeats the M-BA cell, but at the same time has somewhat larger parameters.

Supplementary Materials: The following supporting information can be downloaded at: https://www.mdpi.com/article/10.3390/cryst13091302/s1, Figure S1: EDX analysis of M-BA-TBA crystals; Figure S2. (a) Micrograph of an M-TBA crystal. (b) Fluorescence spectrum of this crystal; Structures and crystallographic information files for M-TBA; Figure S3. CP/MAS and CPPI NMR spectra of M-TBA.; Cartesian atomic coordinates of all model structures as xyz-files.

Author Contributions: Conceptualization, I.V.M. and E.V.S.; Data curation, I.V.M., A.S.N., M.O. and E.V.S.; Formal analysis, I.V.M., V.V.S., P.V.N., M.O., V.V.G. and N.D.O.; Funding acquisition, P.V.N. and E.V.S.; Investigation, I.V.M., V.V.S., P.V.N., M.O. and V.V.G.; Methodology, I.V.M., V.V.S., A.S.N. and N.D.O.; Project administration, I.V.M.; Resources, I.V.M., P.V.N., M.O. and V.V.G.; Software, I.V.M., P.V.N., A.S.N., V.V.G. and N.D.O.; Supervision, I.V.M. and E.V.S.; Validation, I.V.M. and V.V.S.; Visualization, I.V.M., P.V.N. and R.V.S.; Writing—original draft, I.V.M.; Writing—review and editing, I.V.M., P.V.N., A.S.N., R.V.S. and N.D.O. All authors have read and agreed to the published version of the manuscript.

Funding: The work was carried out with the support of the Ministry of Science and Higher Education of the Russian Federation (agreement No 2019-1075) and Priority 2030 Program is acknowledged for Infrastructural Support.

Data Availability Statement: Not applicable.

Acknowledgments: The work was also carried out using computing resources of the federal collective usage center Complex for Simulation and Data Processing for Mega-science Facilities at NRC "Kurchatov Institute". The single crystal XRD studies were performed at the X-ray Diffraction Centre of the St. Petersburg State University. SEM studies were performed at "Geomodel". The authors express their gratitude to the ITMO University Core Facility Center "Nanotechnologies".

Conflicts of Interest: The authors declare no conflict of interest.

References

1. Sherrington, D.C.; Taskinen, K.A. Self-assembly in synthetic macromolecular systems via multiple hydrogen bonding interactions. *Chem. Soc. Rev.* **2001**, *30*, 83–93. [CrossRef]
2. Lenthall, J.T.; Foster, J.A.; Anderson, K.M.; Probert, M.R.; Howard, J.A.K.; Steed, J.W. Hydrogen bonding interactions with the thiocarbonyl π-system. *CrystEngComm* **2011**, *13*, 3202–3212. [CrossRef]
3. Chand, A.; Sahoo, D.K.; Rana, A.; Jena, S.; Biswal, H.S. The Prodigious Hydrogen Bonds with Sulfur and Selenium in Molecular Assemblies, Structural Biology, and Functional Materials. *Acc. Chem. Res.* **2020**, *53*, 1580–1592. [CrossRef] [PubMed]
4. Mundlapati, V.R.; Gautam, S.; Sahoo, D.K.; Ghosh, A.; Biswal, H.S. Thioamide, a Hydrogen Bond Acceptor in Proteins and Nucleic Acids. *J. Phys. Chem. Lett.* **2017**, *8*, 4573–4579. [CrossRef] [PubMed]
5. Li, C.; Hilgeroth, P.; Hasan, N.; Ströhl, D.; Kressler, J.; Binder, W.H. Comparing C2=O and C2=S Barbiturates: Different Hydrogen-Bonding Patterns of Thiobarbiturates in Solution and the Solid State. *Int. J. Mol. Sci.* **2021**, *22*, 12679. [CrossRef]
6. Tsikas, D. Assessment of lipid peroxidation by measuring malondialdehyde (MDA) and relatives in biological samples: Analytical and biological challenges. *Anal. Biochem.* **2017**, *524*, 13–30. [CrossRef]
7. Olyaei, A.; Sadeghpour, M. Barbituric acids in the synthesis of naphthopyranopyrimidines: A brief review. *Synth. Commun.* **2022**, *52*, 2179–2197.
8. Bhatt, R.; Kushwaha, S.; Bojja, S.; Padmaja, P. Chitosan–Thiobarbituric Acid: A Superadsorbent for Mercury. *ACS Omega* **2018**, *3*, 13183–13194. [CrossRef]
9. Jindal, G.; Kaur, N. Barbituric acid appended fluorescent sensor for the detection of Cu^{2+}/Hg^{2+} ions along with real-life utility in recognition of malathionin food samples and fingerprint imaging. *J. Photochem. Photobiol. A Chem.* **2023**, *434*, 114238. [CrossRef]
10. Wang, Y.; Chen, P.; Luo, Q.; Li, X.; Zhu, W. Supramolecular polymeric prodrug micelles for efficient anticancer drug delivery. *Polym. Chem.* **2022**, *13*, 2980–2987. [CrossRef]
11. Brahmachari, G.; Bhowmick, A.; Karmakar, I. Catalyst- and Additive-Free C(sp3)-H Functionalization of (Thio)barbituric Acids via C-5 Dehydrogenative Aza-Coupling under Ambient Conditions. *ACS Omega* **2022**, *7*, 30051–30063. [CrossRef] [PubMed]
12. Chierotti, M.R.; Ferrero, L.; Garino, N.; Gobetto, R.; Pellegrino, L.; Braga, D.; Grepioni, F.; Maini, L. The richest collection of tautomeric polymorphs: The case of 2-thiobarbituric acid. *Chem. A Eur. J.* **2010**, *16*, 4347–4358. [CrossRef] [PubMed]
13. Kadoma, Y.; Fujisawa, S. Radical-scavenging activity of thiols, thiobarbituric acid derivatives and phenolic antioxidants determined using the induction period method for radical olymerization of methyl methacrylate. *Polymers* **2012**, *4*, 1025–1036. [CrossRef]
14. Sharma, A.; Zamisa, S.J.; Noki, S.; Almarhoon, Z.; El-Faham, A.; la Torre, B.G.d.; Albericio, F. Crystal structure, spectroscopic studies and theoretical studies of thiobarbituric acid derivatives: Understanding the hydrogen-bonding patterns. *Acta Crystallogr. Sect. C Struct. Chem.* **2018**, *74*, 1703–1714. [CrossRef] [PubMed]
15. Emara, R.; Masoud, M.S.; Abboudy, S. Optical, electrical, thermal and kinetic studies for some pyrimidine ligands and their complexes. *J. Non. Cryst. Solids* **2022**, *597*, 121873. [CrossRef]
16. Mahmudov, K.T.; Kopylovich, M.N.; Maharramov, A.M.; Kurbanova, M.M.; Gurbanov, A.V.; Pombeiro, A.J.L. Barbituric acids as a useful tool for the construction of coordination and supramolecular compounds. *Coord. Chem. Rev.* **2014**, *265*, 1–37. [CrossRef]
17. Aizawa, T.; Kawaura, M.; Kajitani, T.; Hengphasatporn, K.; Shigeta, Y.; Yagai, S. Supramolecular polymerization of thiobarbituric acid naphthalene dye. *Chem. Commun.* **2022**, *58*, 9365–9368. [CrossRef] [PubMed]

18. Kawaura, M.; Aizawa, T.; Takahashi, S.; Miyasaka, H.; Sotome, H.; Yagai, S. Fluorescent supramolecular polymers of barbiturate dyes with thiophene-cored twisted π-systems. *Chem. Sci.* **2022**, *13*, 1281–1287. [CrossRef]
19. Hützler, W.M.; Bolte, M. Sulfur as hydrogen-bond acceptor in cocrystals of 2-thio-modified thymine. *Acta Crystallogr. Sect. C Struct. Chem.* **2018**, *74*, 21–30. [CrossRef]
20. Marshall, M.G.; Lopez-Diaz, V.; Hudson, B.S. Single-Crystal X-ray Diffraction Structure of the Stable Enol Tautomer Polymorph of Barbituric Acid at 224 and 95 K. *Angew. Chem.* **2016**, *128*, 1331–1334. [CrossRef]
21. Grześkiewicz, A.M.; Kubicki, M. Two Tautomers of Thiobarbituric Acid in One Crystal: The Experimental Charge Density Perspective. *Materials* **2021**, *15*, 223. [CrossRef]
22. Méndez, E.; Cerdá, M.F.; Gancheff, J.S.; Torres, J.; Kremer, C.; Castiglioni, J.; Kieninger, M.; Ventura, O.N. Tautomeric forms of 2-thiobarbituric acid as studied in the solid, in polar solutions, and on gold nanoparticles. *J. Phys. Chem. C* **2007**, *111*, 3369–3383. [CrossRef]
23. Liu, X.; Huang, D.; Lai, C.; Zhang, C.; Qin, L.; Li, B.; Yi, H.; Deng, R.; Liu, S.; Zhang, M.; et al. Visual Method for Selective Detection of Hg^{2+}Based on the Competitive Interactions of 2-Thiobarbituric Acid with Au Nanoparticles and Hg^{2+}. *ACS Appl. Nano Mater.* **2021**, *4*, 6760–6767. [CrossRef]
24. Orekhov, N.; Kondratyuk, N.; Logunov, M.; Timralieva, A.; Shilovskikh, V.; Skorb, E. V Insights into the Early Stages of Melamine Cyanurate Nucleation from Aqueous Solution. *Cryst. Growth Des.* **2021**, *21*, 1984–1992. [CrossRef]
25. Petelski, A.N.; Duarte, D.J.R.; Pamies, S.C.; Peruchena, N.M.; Sosa, G.L. Intermolecular perturbation in the self-assembly of melamine. *Theor. Chem. Acc.* **2016**, *135*, 65. [CrossRef]
26. Gus'kov, V.Y.; Sukhareva, D.A.; Gainullina, Y.Y.; Hamitov, E.M.; Galkin, Y.G.; Maistrenko, V.N. Chiral recognition capabilities of melamine and cyanuric acid supramolecular structures. *Supramol. Chem.* **2018**, *30*, 940–948. [CrossRef]
27. Aliev, T.A.; Timralieva, A.A.; Kurakina, T.A.; Katsuba, K.E.; Egorycheva, Y.A.; Dubovichenko, M.V.; Kutyrev, M.A.; Shilovskikh, V.V.; Orekhov, N.; Kondratyuk, N.; et al. Designed assembly and disassembly of DNA in supramolecular structure: From ion regulated nuclear formation and machine learning recognition to running DNA cascade. *Nano Sel.* **2022**, *3*, 1526–1536. [CrossRef]
28. Shilovskikh, V.V.; Timralieva, A.A.; Belogub, E.V.; Konstantinova, E.A.; Kokorin, A.I.; Skorb, E. V Radical Activity of Binary Melamine-Based Hydrogen-Bonded Self-Assemblies. *Appl. Magn. Reson.* **2020**, *51*, 939–949. [CrossRef]
29. Nesterov, P.V.; Shilovskikh, V.V.; Sokolov, A.D.; Gurzhiy, V.V.; Novikov, A.S.; Timralieva, A.A.; Belogub, E.V.; Kondratyuk, N.D.; Orekhov, N.D.; Skorb, E.V. Encapsulation of Rhodamine 6G Dye Molecules for Affecting Symmetry of Supramolecular Crystals of Melamine-Barbiturate. *Symmetry* **2021**, *13*, 1119. [CrossRef]
30. Shilovskikh, V.V.; Timralieva, A.A.; Nesterov, P.V.; Novikov, A.S.; Sitnikov, P.A.; Konstantinova, E.A.; Kokorin, A.I.; Skorb, E. V Melamine—Barbiturate Supramolecular Assembly as a pH-Dependent Organic Radical Trap Material. *Chem. Eur. J.* **2020**, *26*, 16603–16610. [CrossRef]
31. Timralieva, A.A.; Moskalenko, I.V.; Nesterov, P.V.; Shilovskikh, V.V.; Novikov, A.S.; Konstantinova, E.A.; Kokorin, A.I.; Skorb, E. V Melamine Barbiturate as a Light-Induced Nanostructured Supramolecular Material for a Bioinspired Oxygen and Organic Radical Trap and Stabilization. *ACS Omega* **2023**, *8*, 8276–8284. [CrossRef] [PubMed]
32. Alabusheva, V.S.; Shilovskikh, V.V.; Bridenko, L.A.; Gurzhiy, V.V.; Skorb, E.V. Synthesis of Catalytic Microswimmers Based on Anisotropic Platinum Sorption on Melamine Barbiturate Supramolecular Structures. *Adv. Intell. Syst.* **2023**, *5*, 2200436. [CrossRef]
33. Prior, T.J.; Armstrong, J.A.; Benoit, D.M.; Marshall, K.L. The structure of the melamine-cyanuric acid co-crystal. *CrystEngComm* **2013**, *15*, 5838–5843. [CrossRef]
34. Rigaku Oxford Diffraction. *CrysAlisPro Software System*, version 1.171.38.46; Rigaku Oxford Diffraction: Oxford, UK, 2015.
35. Sheldrick, G.M. SHELXT—Integrated space-group and crystal-structure determination. *Acta Crystallogr. Sect. A Found. Crystallogr.* **2015**, *A71*, 3–8. [CrossRef]
36. Sheldrick, G.M. Crystal structure refinement with SHELXL. *Acta Crystallogr. Sect. C Struct. Chem.* **2015**, *C71*, 3–8. [CrossRef] [PubMed]
37. Dolomanov, O.V.; Bourhis, L.J.; Gildea, R.J.; Howard, J.A.K.; Puschmann, H. OLEX2: A complete structure solution, refinement and analysis program. *J. Appl. Crystallogr.* **2009**, *42*, 339–341. [CrossRef]
38. Neese, F. The ORCA program system. *Wiley Interdiscip. Rev. Comput. Mol. Sci.* **2012**, *2*, 73–78. [CrossRef]
39. Neese, F.; Wennmohs, F.; Hansen, A.; Becker, U. Efficient, approximate and parallel Hartree-Fock and hybrid DFT calculations. A "chain-of-spheres" algorithm for the Hartree-Fock exchange. *Chem. Phys.* **2009**, *356*, 98–109. [CrossRef]
40. Neese, F. An Improvement of the Resolution of the Identity. *J. Comput. Chem.* **2003**, *24*, 1740–1747. [CrossRef]
41. Marenich, A.V.; Cramer, C.J.; Truhlar, D.G. Universal solvation model based on solute electron density and on a continuum model of the solvent defined by the bulk dielectric constant and atomic surface tensions. *J. Phys. Chem. B* **2009**, *113*, 6378–6396. [CrossRef]
42. Berendsen, H.J.C.; van der Spoel, D.; van Drunen, R. GROMACS: A message-passing parallel molecular dynamics implementation. *Comput. Phys. Commun.* **1995**, *91*, 43–56. [CrossRef]
43. Jorgensen, W.L.; Maxwell, D.S.; Tirado-Rives, J. Development and testing of the OPLS all-atom force field on conformational energetics and properties of organic liquids. *J. Am. Chem. Soc.* **1996**, *118*, 11225–11236. [CrossRef]
44. Dodda, L.S.; De Vaca, I.C.; Tirado-Rives, J.; Jorgensen, W.L. LigParGen web server: An automatic OPLS-AA parameter generator for organic ligands. *Nucleic Acids Res.* **2017**, *45*, W331–W336. [CrossRef] [PubMed]

45. Jorgensen, W.L.; Tirado-Rives, J. Potential energy functions for atomic-level simulations of water and organic and biomolecular systems. *Proc. Natl. Acad. Sci. USA* **2005**, *102*, 6665–6670. [CrossRef]
46. Jorgensen, W.L.; Chandrasekhar, J.; Madura, J.D.; Impey, R.W.; Klein, M.L. Comparison of simple potential functions for simulating liquid water. *J. Chem. Phys.* **1983**, *79*, 926–935. [CrossRef]
47. Essmann, U.; Perera, L.; Berkowitz, M.L.; Darden, T.; Lee, H.; Pedersen, L.G. A smooth particle mesh Ewald method. *J. Chem. Phys.* **1995**, *103*, 8577–8593. [CrossRef]
48. Brehm, M.; Kirchner, B. TRAVIS—A free analyzer and visualizer for monte carlo and molecular dynamics trajectories. *J. Chem. Inf. Model.* **2011**, *51*, 2007–2023. [CrossRef] [PubMed]
49. Delchev, V.B. DFT ab initio study of the keto-enol tautomerism of barbituric acid. *J. Struct. Chem.* **2004**, *45*, 570–578. [CrossRef]
50. Nemes, C.T.; Laconsay, C.J.; Galbraith, J.M. Hydrogen bonding from a valence bond theory perspective: The role of covalency. *Phys. Chem. Chem. Phys.* **2018**, *20*, 20963–20969. [CrossRef]
51. Karas, L.J.; Wu, C.H.; Das, R.; Wu, J.I.C. Hydrogen bond design principles. *Wiley Interdiscip. Rev. Comput. Mol. Sci.* **2020**, *10*, e1477. [CrossRef]
52. Khitrov, M.D.; Platonov, D.N.; Belyy, A.Y.; Trainov, K.P.; Velmiskina, J.A.; Medvedev, M.G.; Salikov, R.F.; Tomilov, Y.V. A unique small molecule class of fluorophores with large Stokes shift based on the electron deficient 9-methoxypyrroloisoquinolinetrione core. *Dye. Pigment.* **2022**, *203*, 110344. [CrossRef]
53. Huang, J.; Yang, L.; Fu, M.; Chen, Z.; Huang, X. Theoretical investigations on the excited-state intramolecular proton transfer in the solvated 2-hydroxy-1-naphthaldehyde carbohydrazone. *Open Chem.* **2022**, *20*, 785–792. [CrossRef]
54. Mrad, R.; Poggi, M.; Ben Chaâbane, R.; Negrerie, M. Role of surface defects in colloidal cadmium selenide (CdSe) nanocrystals in the specificity of fluorescence quenching by metal cations. *J. Colloid Interface Sci.* **2020**, *571*, 368–377. [CrossRef] [PubMed]
55. Stevens, J.S.; Byard, S.J.; Schroeder, S.L.M. Characterization of Proton Transfer in Co-Crystals by X-ray Photoelectron Spectroscopy (XPS). *Cryst. Growth Des.* **2010**, *10*, 1435–1442. [CrossRef]
56. Stevens, J.S.; Byard, S.J.; Seaton, C.C.; Sadiq, G.; Davey, R.J.; Schroeder, S.L.M. Proton transfer and hydrogen bonding in the organic solid state: A combined XRD/XPS/ssNMR study of 17 organic acid-base complexes. *Phys. Chem. Chem. Phys.* **2014**, *16*, 1150–1160. [CrossRef]

Disclaimer/Publisher's Note: The statements, opinions and data contained in all publications are solely those of the individual author(s) and contributor(s) and not of MDPI and/or the editor(s). MDPI and/or the editor(s) disclaim responsibility for any injury to people or property resulting from any ideas, methods, instructions or products referred to in the content.